PAPER • OPEN ACCESS

Revealing orbital and magnetic phase transitions in $Pr_{0.5}Ca_{0.5}MnO_3$ epitaxial thin films by resonant soft x-ray scattering

To cite this article: H Wadati *et al* 2014 *New J. Phys.* **16** 033006

New Journal of Physics
The open access journal at the forefront of physics
Deutsche Physikalische Gesellschaft DPG | IOP Institute of Physics

Revealing orbital and magnetic phase transitions in $Pr_{0.5}Ca_{0.5}MnO_3$ epitaxial thin films by resonant soft x-ray scattering

H Wadati[1,2], J Geck[3], E Schierle[4], R Sutarto[1,5], F He[5], D G Hawthorn[6], M Nakamura[7], M Kawasaki[2,7], Y Tokura[2,7] and G A Sawatzky[1]

[1] Department of Physics and Astronomy, University of British Columbia, Vancouver, British Columbia, Canada V6T 1Z1
[2] Department of Applied Physics and Quantum-Phase Electronics Center (QPEC), University of Tokyo, Hongo, Tokyo 113-8656, Japan
[3] Leibniz Institute for Solid State and Material Research IFW Dresden, Helmholtzstrasse 20, D-01069 Dresden, Germany
[4] Helmholtz-Zentrum Berlin fur Materialien und Energie Albert-Einstein-Strasse 15, D-12489 Berlin, Germany
[5] Canadian Light Source, University of Saskatchewan, Saskatoon, Saskatchewan, Canada S7N 2V3
[6] Department of Physics and Astronomy, University of Waterloo, Waterloo, Ontario, Canada N2L 3G1
[7] RIKEN Center for Emergent Matter Science (CEMS), Wako 351-0198, Japan
E-mail: wadati@ap.t.u-tokyo.ac.jp

Received 5 November 2013, revised 27 January 2014
Accepted for publication 4 February 2014
Published 5 March 2014

New Journal of Physics **16** (2014) 033006
doi:10.1088/1367-2630/16/3/033006

Abstract

We report the study of magnetic and orbital order in $Pr_{0.5}Ca_{0.5}MnO_3$ epitaxial thin films grown on $(LaAlO_3)_{0.3}$–$(SrAl_{0.5}Ta_{0.5}O_3)_{0.7}$. Resonant soft x-ray scattering revealed significant modifications of the magnetic order in the film as compared to the bulk. Namely (i) a different magnetic ordering wave vector, (ii) different spin directions and (iii) an additional magnetic reordering transition. We demonstrate that an analysis of the resonant scattering which is based solely on local symmetries and which does not involve a modeling of energy-dependent lineshapes allows to extract this detailed microscopic information. This approach significantly simplifies the analysis and interpretation of resonant scattering data.

Keywords: resonant soft x-ray scattering, $Pr_{0.5}Ca_{0.5}MnO_3$, thin films, phase transitions, orbital ordering, magnetic ordering

1. Introduction

Hole-doped perovskite manganites $R_{1-x}A_xMnO_3$, where R is a rare-earth (R = La, Nd, Pr) and A is an alkaline-earth atom (A = Sr, Ba, Ca) have attracted much attention because they exhibit remarkable physical properties such as colossal magnetoresistance and complex electronic ordering phenomena [1–8]. For the latter, the half-doped manganites provide a particularly prominent and extensively studied example, namely the so-called CE-phase [9]. This phase is commonly discussed in terms of cooperative spin, charge and orbital order, where ferromagnetic zig-zag chains are formed, which are coupled antiferromagnetically to each other. Although the detailed microscopic structure of this electronic order remains to be fully understood [10, 11], it is clear that it couples strongly to the lattice via the orbital degree of freedom. Epitaxially strained thin films thus enable one to tune the electronic ordering properties in the doped manganites and to engineer their electronic properties. It is therefore very important to investigate and understand the electronic modifications in doped manganite films, which can be dramatic. For example, it was recently shown that epitaxial strain effects can control charge ordering (CO) in thin films of Mn oxides [12, 13]. A transition between CO and ferromagnetic metallic states was observed in $Nd_{0.5}Sr_{0.5}MnO_3$ films on $SrTiO_3$ $(011)_c$ substrates, whereas $Nd_{0.5}Sr_{0.5}MnO_3$ films on $SrTiO_3(001)_c$ substrates exhibit only insulating behavior at all temperatures [12]. Here the substrate orientation is given in the standard cubic notation as indicated by the subscript c. Also in $Pr_{0.5}Ca_{0.5}MnO_3$ thin films, epitaxial strain strongly affects the electronic properties. Previous studies have shown that $Pr_{0.5}Ca_{0.5}MnO_3$ films grown epitaxially on $(LaAlO_3)_{0.3}$–$(SrAl_{0.5}Ta_{0.5}O_3)_{0.7}$(LSAT) $(011)_c$ substrate exhibit a CO transition around 220 K, similar to bulk samples, while $Pr_{0.5}Ca_{0.5}MnO_3$ films on LSAT $(001)_c$ substrates have a much higher CO transition temperature around 300 K [13].

Here we present a resonant soft x-ray scattering (RSXS) study of the electronic order in $Pr_{0.5}Ca_{0.5}MnO_3$ thin films grown epitaxially on LSAT $(011)_c$. RSXS at the Mn $2p$ edge has been shown to provide a unique means to study ordered states in Mn oxides [14–20]. Non-resonant x-ray scattering is dominated by charge scattering and the relative intensity of magnetic scattering to charge scattering is $(\hbar\omega/m_ec^2)^2 \sim 10^{-4}$, where $\hbar\omega$ is the x-ray energy and m_ec^2 is the electron mass. In RSXS one can obtain a strong magnetic signal by using a large spin-orbit splitting (~10 eV) in $2p$ core levels of the $3d$ transition metals. This technique is especially suitable for studying the magnetic structures in small samples due to the large resonant enhancement and the high photon flux at present synchrotron radiation sources. Consequently it has been successfully applied to reveal the magnetic orderings in thin films of non-collinear magnetic $NdNiO_3$ [21] and multiferroic $YMnO_3$ [20]. Our results show that the microscopic magnetic order in films can differ significantly from that of the corresponding bulk materials, and indicate that epitaxial strain couples to the spin order via the orbital degrees of freedom, which provides a potential route towards tuning the magnetic properties of doped manganite films.

2. Experiment

$Pr_{0.5}Ca_{0.5}MnO_3$ thin films with the thickness of 40 nm were grown on LSAT $(011)_c$ substrates by pulsed laser deposition. Details of the fabrication and characterization of the thin films were described elsewhere [13]. RSXS experiments at the Mn 2*p* edge were performed at the BESSY undulator beamline UE46-PGM1 and 10ID-2 (REIXS) of the Canadian Light Source [22] in a horizontally scattering geometry. Scattering spectra were measured using horizontally (π) or vertically (σ) polarized light. We will refer to the resonant intensity measured in the $\pi \rightarrow \sigma'$, π' and $\sigma \rightarrow \sigma'$, π' channels as I_π and I_σ, respectively (primes denote the polarization of the scattered x-rays). The pressure during measurements was below 5×10^{-9} Torr, and the temperature was varied between room temperature and 25 K. We also performed x-ray absorption spectroscopy (XAS) measurements in the total-electron-yield mode.

In the following, the (*HKL*) indexes for the film reflections and directions refer to the orthorhombic unit cell of the $Pr_{0.5}Ca_{0.5}MnO_3$ thin film [13]. At this point it is important to realize that the $Pr_{0.5}Ca_{0.5}MnO_3$ thin films contain structural domains with interchanged *a*- and *b*-axes—so-called twin domains. We will refer to these twin domains as *D*1 and *D*2, respectively, and designate the reflections and directions of these domains with a corresponding index. Using this convention, the orthorhombic $(100)_{D1}$ and $(011)_{D1}$ directions were parallel to the scattering plane as shown in figure 1(a), which corresponds to $(010)_{D2}$ and $(101)_{D2}$ of the other twin domain. The coexistence of the domains *D*1 and *D*2 is also shown in figure A1 of appendix A. In a scattering experiment, the diffraction patterns of *D*1 and *D*2 are superimposed. This means that close to the position of $(H, 0, 0)_{D1}$, the $(0, H, 0)_{D2}$ reflection can be observed, if it occurs as well. However, because $a \neq b$, these two reflections possess slightly different scattering angles. This orthorhombic peak splitting allows the identification of $(H, 0, 0)_{D1}$ and $(0, H, 0)_{D2}$ reflections from the different domains.

3. Results and discussion

Figure 1(c) shows the temperature dependence of the resonant intensity measured around the $(1/2, 0, 0)_{D1}$ position with incoming π-polarization. The photon energy was set to 643.6 eV, which corresponds to the Mn 2*p* absorption peak (cf appendix). RSXS intensity appears around 210 K and strongly gains intensity with decreasing temperature. This result is in good agreement with the charge/orbital-ordering transition temperature $T_{CO/OO} = 220$ K reported in [13].

The position of the superlattice peak as a function of temperature is shown in figure 1(d). A clear shift of the peak position is observed at the magnetic ordering temperature $T_N = 150$ K, even though the lattice parameters do not change significantly at this temperature [13]. Above T_N and below $T_{CO/OO}$, the peak position corresponds exactly to the $(1/2, 0, 0)_{D1}$ reflection, identifying it as the superlattice reflection due to the orbital order in *D*1. Note that the orbital order causes a doubling of the orthorhombic *a*-axis only, i.e. the $(0, 1/2, 0)_{D2}$ does not occur in the orbital ordered phase. However, with the onset of magnetic order below T_N, the peak position jumps to $(0, 1/2, 0)_{D2}$, implying that the observed intensity is now due to the magnetic order in twin domain *D*2. As we will discuss further below, the orbital scattering of *D*1 still exists below T_N, but its intensity is much smaller than the magnetic scattering of *D*2. We can

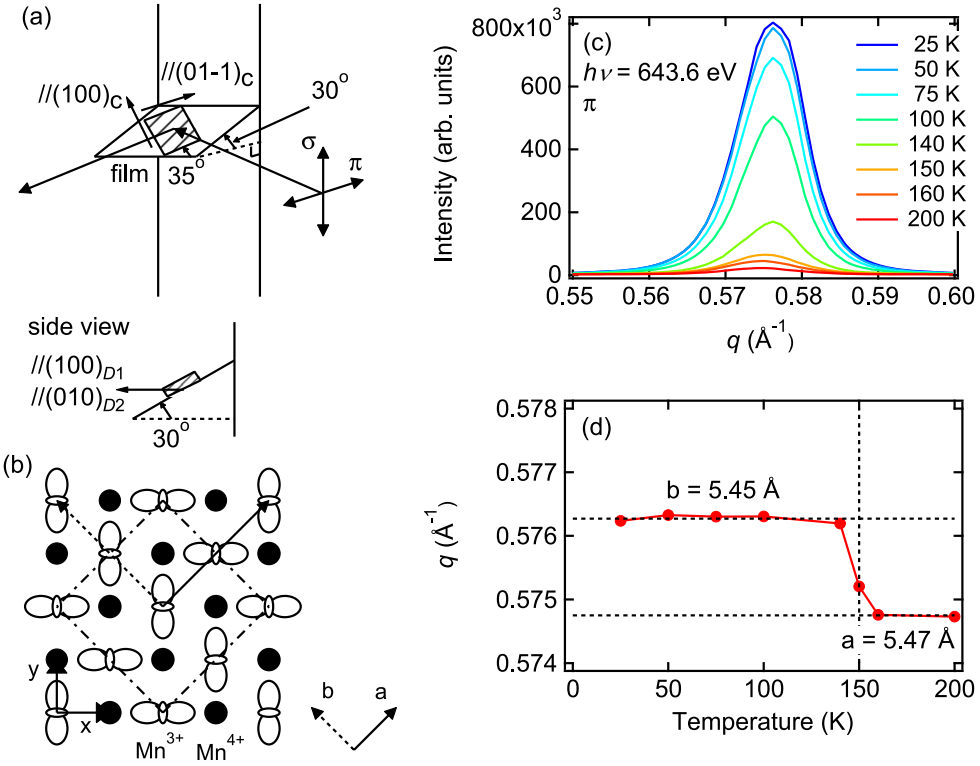

Figure 1. Temperature dependence observed at the $(1/2, 0, 0)_{D1}$ position (c). The experimental geometry is shown in panel (a). Panel (b) shows the schematic drawing of the charge-orbital ordering. The arrow marks the directions for the orbital ordering and the dashed arrow for the spin ordering. Panel (d) shows the peak positions as a function of temperature.

also exclude non-collinear or incommensurate spin arrangements because the observed shift in figure 1(d) is simply due to the different domains with different lattice constants.

The peak widths in figure 1(c) do not show much temperature dependence with almost constant full width at half maximum Δq of 0.01 Å^{-1}. This gives a common correlation length $\xi = 2\pi/\Delta q \sim 60$ nm of the orbital order along a and the magnetic order along b, which are both comparable to the thickness of the thin film.

Figure 2 shows the photon-energy dependence of the intensity observed at the $(1/2, 0, 0)_{D1}$ position across the Mn $2p$ edges at various temperatures using π and σ polarizations. To facilitate a comparison of the lineshapes, panels (c) and (d) show the same data as given in (a) and (b), but this time normalized to the area. As can be observed in figure 2, I_π and I_σ are of very similar magnitude and exhibit the same lineshapes for 150 K $< T <$ 200 K, i.e. $I_\pi \simeq I_\sigma$ for the orbital $(1/2, 0, 0)_{D1}$ peak. These lineshapes are reminiscent to that of corresponding bulk materials [14, 15, 17], supporting interpretation in terms of orbital ordering. However, the present data for the film display differences from those for the bulk, indicative of a modified orbital state. The condition $I_\pi \simeq I_\sigma$ clearly breaks down at 150 K upon cooling: while I_π shows a strong increase by a factor of $\sim$10 accompanied by a clear lineshape change, I_σ remains almost unaltered. Furthermore, whereas the peak in I_π apparently shifts in position, as described above (cf figure 1), the peak in I_σ does not move at T_N. Since the additional scattering from $D2$ sets in

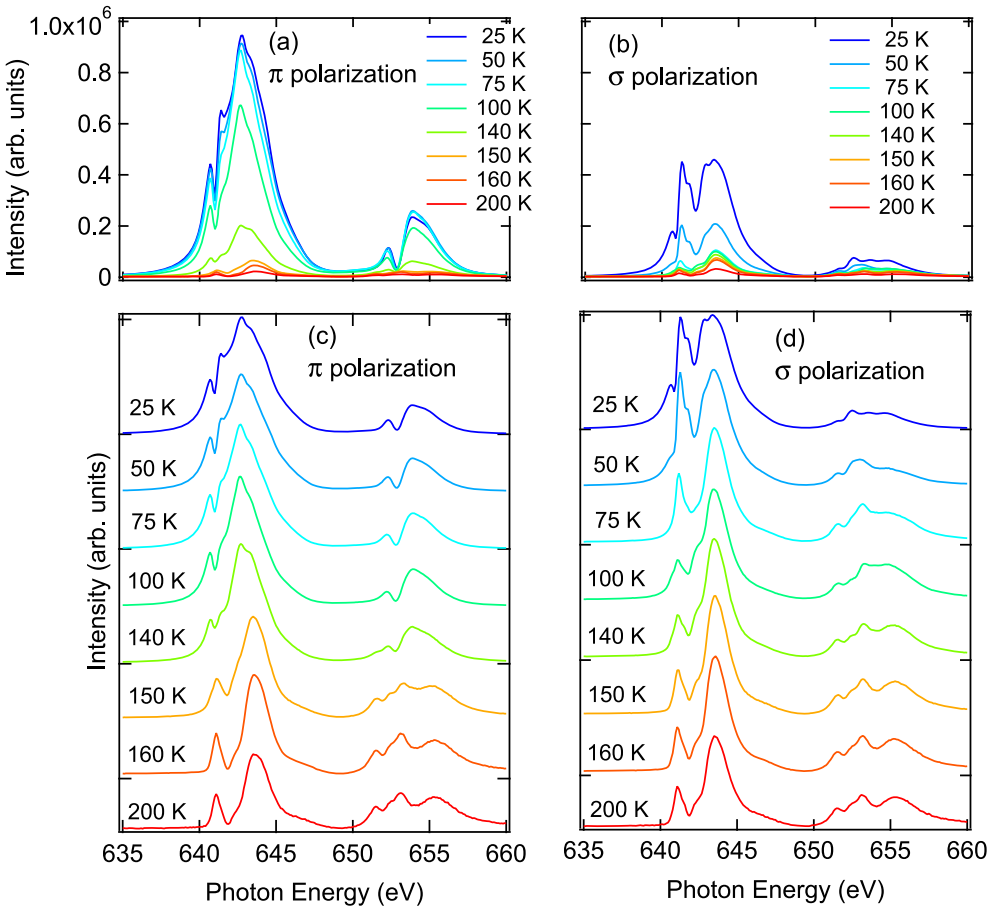

Figure 2. Photon-energy dependence of the (1/2, 0, 0)|(0, 1/2, 0) peak intensity at Mn $2p$ edges at various temperatures using π polarization (a) and σ polarization (b). To compare lineshapes, all data in the panels (a) and (b) have been normalized to each spectrum area, shown at the respective panels (c) and (d) as a function of photon energies.

at T_N, we conclude that it is resonant magnetic scattering of the Mn-sublattice, which corresponds to $(0, 1/2, 0)_{D2}$ of $D2$. Interestingly, the magnetic signal is almost entirely restricted to I_π, whereas I_σ is due to the orbital $(1/2, 0, 0)_{D1}$ peak of $D1$.

We observe another dramatic change of the RSXS linshapes at $T_2 = 75$ K well below T_N. This time, I_σ displays clear changes of lineshape and intensity, as shown in figures 2(b) and (d). The variation of I_σ across T_2 signals a third phase transition, which has not been reported earlier and is absent in the bulk material. We also note that the resonant magnetic scattering of the film exhibits a lineshape, which is very different from that of related bulk materials [17].

The phase transitions at T_N and T_2 are also clearly revealed by the data presented in figure 3(a), which shows I_π and I_σ integrated over the Mn $2p_{3/2}$ and $2p_{1/2}$ regions. One can see a large increase of the total scattering intensity by a factor of more than 10 in I_π around 150 K. This demonstrates the sensitivity of the RSXS-intensity in going from orbital to orbital plus spin order. I_σ increases strongly around $T_2 = 75$ K.

Following the approach of earlier studies [15, 17], we plot the so-called branching ratio as a function of temperature in figure 3(b), which makes the changes at T_N and T_2 even more apparent. Branching ratios are defined by the intensity contributions from the Mn $2p_{3/2}$ region

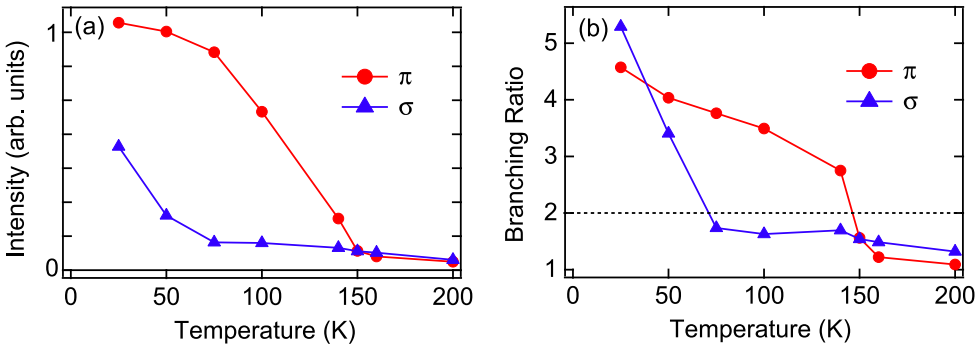

Figure 3. The integrated intensities of the (1/2, 0, 0)|(0, 1/2, 0) peak over both the Mn $2p_{3/2}$ and Mn $2p_{1/2}$ regions (a) and the branching ratio (b), where a statistical value of 2 is also indicated by the dash line.

divided by that from the Mn $2p_{1/2}$ region [23]. The branching ratios change strongly around 150 K for a π polarization, and similarly around 75 K for a σ polarization. An anomaly of the branching ratio was also reported at T_N in the orbital-ordered peak of layered manganites $La_{0.5}Sr_{1.5}MnO_4$ [17], but the anomaly is much smaller, and it is related to T_N while the large anomaly we observe is well below T_N and so has a very different origin. Note that the existence of these phase transitions was not observed by macroscopic measurements (see the appendix), showing the advantage of RSXS for studying the magnetic structures in thin films.

In order to gain a better understanding of the experimental results, we have investigated the resonant structure factor F at the Mn $2p$ edges. Referring to the standard model of the CE-phase, we describe the so-called Mn^{3+} sites within a local D_{4h}-symmetry, which corresponds to the occupied orbital, while the local symmetry of the so-called Mn^{4+} sites is taken to be O_h (cf figure 1 and the appendix). Note, that the present model refers to local symmetries only and does not make any assumptions regarding the charge disproportionation in the CE-phase.

The resonant scattering length of a given site n can be expressed as $f_n = \mathbf{e}_f^+ \cdot \hat{f}_n(\hbar\omega, \hat{s}) \cdot \mathbf{e}_i$, with $\hbar\omega$ the photon energy, $\hat{s} = (s_x, s_y, s_z)$ the direction of the local spin, and $\mathbf{e}_i(\mathbf{e}_f)$ the polarization of the incident (scattered) beam. For the $\hat{f}_n$ in O_h and D_{4h} we use formulae given in [24], which express the (3 × 3)-matrixes $\hat{f}_n$ in terms of a few fundamental spectra $f_{n,j}^{(k)}(\hbar\omega)$ with $k = 0, 1, 2, 3$. At the Mn $2p$ resonance, the scattering is completely dominated by the Mn-sublattice. We therefore calculate the resonant structure factor matrix $\hat{F}(\mathbf{Q}) = \sum_n \hat{f}_n \exp(i\mathbf{Q} \cdot \mathbf{r}_n) = \sum_{k=0}^{3} \hat{F}^{(k)}(\mathbf{Q})$ by summing over the 16 Mn sites of the CE-supercell. Here, $\hat{F}^{(k)}$ only contains fundamental spectra with fixed k. The scattering amplitude and intensity for given $\mathbf{e}_i$ and $\mathbf{e}_f$ can then be calculated as $A_{if} = \mathbf{e}_i^+ \cdot \hat{F} \cdot \mathbf{e}_f$ and $I_{if} \propto |A_{if}|^2$, respectively.

For $T_{CO/OO} > T > T_N$, i.e. for orbital order without spin order, the calculated scattering amplitudes of the orbital (1/2, 0, 0) reflection are $A_{\sigma\sigma'}^{orb} = A_{\pi\pi'}^{orb} = 0$ and $A_{\sigma\pi'}^{orb} = A_{\pi\sigma'}^{orb} \propto (f_{a_{1g},x}^{(0)} - f_{a_{1g},y}^{(0)})$, where $f_{a_{1g},x}^{(0)}$ and $f_{a_{1g},y}^{(0)}$ are fundamental spectra with $k = 0$. These spectra describe the anisotropy with respect to the local C_4-axis in D_{4h}, i.e. the anisotropy for polarizations along or perpendicular to the occupied orbital at the Mn^{3+} sites. The calculation

gives $\sigma\pi'$- and $\pi\sigma'$-scattering only and yields $I_\pi = I_\sigma$, which is identical to previous results and in good agreement with the present experiment.

A more interesting situation arises when orbital and magnetic order coexist ($T < T_N$). As discussed above, the shift in position accompanying the increase of I_π implies that the additional intensity has to be attributed to the magnetic (0, 1/2, 0) superlattice peak. The structure factor of this magnetic reflection is given by $\hat{F}_{mag} = \hat{F}^{(1)}_{mag}(\hat{s}) + \hat{F}^{(3)}_{mag}(\hat{s})$· These terms are related to the circular magnetic dichroism in XAS [24], i.e. the (0, 1/2, 0) reflection is given by terms odd in $\hat{s}$ as it should be.

Comparing F_{orb} and F_{mag} to the experimental data a number of important conclusions can be drawn: since the orbital scattering in I_σ due to the $(1/2, 0, 0)_{D1}$ peak does not change much for $T_2 < T < T_{CO/OO}$, it is still dominated by the same fundamental spectra $f^{(0)}_{a_{1g},x}$ and $f^{(0)}_{a_{1g},y}$ at these temperatures. In contrast to this, the lineshape in I_π does change dramatically with the onset of magnetic order, due to the strong additional magnetic intensity stemming from the $(0, 1/2, 0)_{D2}$ peak. The changed lineshape is easily explained qualitatively by the different fundamental spectra, which enter $\hat{F}_{orb}$ and $\hat{F}_{mag}$.

Furthermore, the experimental results show that for $T_N > T > T_2$ the magnetic intensity is almost exclusively confined to I_π, while there is almost no magnetic scattering in I_σ. This very specific feature of the magnetic scattering provides information about the spin directions in this temperature range: we first note that, since $\left|f^{(k=3)}_{n,j}\right| \ll \left|f^{(k=1)}_{n,j}\right|$ (cf [24]), we can take the approximation $\hat{F} = \hat{F}^{(1)}$, which yields (see the appendix)

$$\begin{aligned}\sqrt{3}\, A^{mag}_{\sigma\pi'} &= f^{(1)}_{a_{2u}}\left((2+3\sqrt{2})\,s_x + (3\sqrt{2}-2)\,s_y\right) \\ &\quad + f^{(1)}_{e_u}\left((2+3\sqrt{2})\,s_x + (3\sqrt{2}-2)\,s_y + 4s_z\right)\end{aligned}$$

$s_{x,y,z}$ refer to the x-, y-, z-axes indicated in figure 1. No magnetic scattering in I_σ means that $A^{mag}_{\sigma\pi'} = 0$ at all photon energies. Since $f^{(1)}_{a_{2u}}$ and $f^{(1)}_{e_u}$ are linearly independent, their coefficients must vanish, which implies that $s_z = 0$ and $s_y/s_x = (2+3\sqrt{2})/(2-3\sqrt{2})$ and corresponds to an easy axis close to $\hat{s}_0 = (\cos\phi,\ \sin\phi,\ 0)$ with $\phi = 110°$. Note that the spin orientation determines how the different fundamental spectra contribute to the total intensity. In other words, the RSXS lineshape of I_σ and I_π depends strongly on the directions of the ordered spins. From this we conclude that the dramatic changes of I_σ below T_2 are due to a spin reorientation, which results in $A_{\sigma\pi'} \neq 0$.

4. Summary

In summary, we performed RSXS studies of the orbital and magnetic order in $Pr_{0.5}Ca_{0.5}MnO_3$ thin films grown on LSAT $(011)_c$ substrates. The different scattering angles together with the polarization and energy-dependent lineshapes enable us to separate the orbital and magnetic scattering originating from different twin domains. We find clear differences between the half doped bulk materials and the studied film samples: (i) the magnetic (0, 1/2, 0) modulation of the

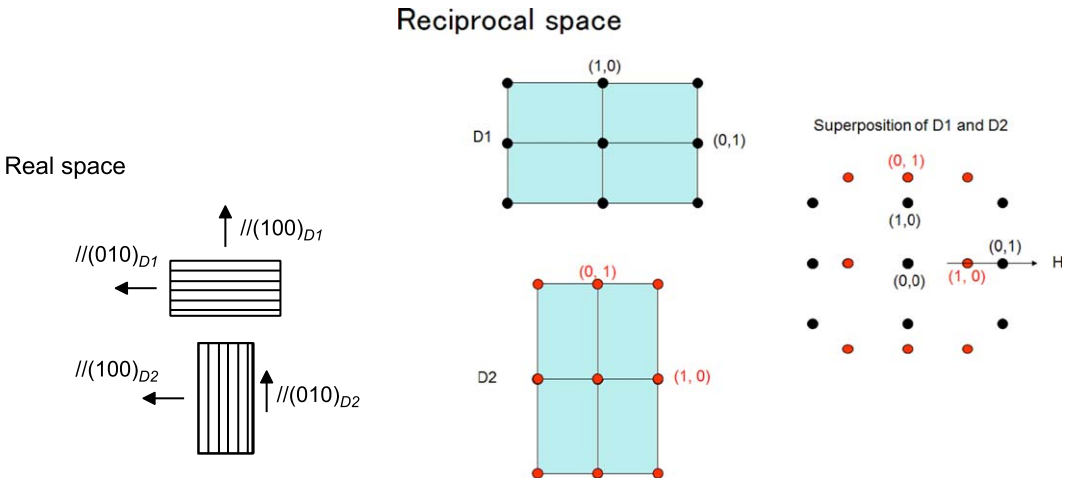

Figure A1. Coexistence of the domains $D1$ and $D2$. The left panel corresponds to real space, whereas the right panels correspond to reciprocal space.

thin film is different from the (0, 1/2, 1) modulation observed for the bulk CE-phase. In contrast to the bulk materials, the film exhibits ferromagnetic spin correlations along the c-axis. (ii) We observe an additional spin reorientation transition at T_2. These modifications of the magnetic structure of the PCMO film might be a result of the epitaxial strain. However, we cannot exclude slight deviations in the stoichiometry away from half doping, which could have similar effects [9].

Nonetheless, our study demonstrates that RSXS combined with an analysis based on solely local symmetries allows to extract detailed microscopic information about electronic order even in thin film samples. Specifically, we not only determine the magnetic ordering wave vector, but also learn about the spin directions by using this symmetry-based approach. The direct relationship between the RSXS lineshape and the spin orientation is new and will surely be very useful in future analyses and theoretical studies.

Even more information, however, could be extracted from a detailed lineshape analysis, and this is also expected to answer the question of the exact nature of the ordered states as proposed in [10, 11]. On the one hand, the present study clearly shows that such a spectral shape analysis obviously cannot be done in the simple and much used spherical approximation, in which the non-spherical local symmetry of the scatterers in a crystalline environment is neglected. On the other hand, a full calculation including the local spin, orbital, and charge as well as the local hybridization with the O orbitals and probably more than a single Mn site in a cluster [25] leads to a rather complicated problem. This is why the above analysis, which is based only on symmetries and selection rules, is so important.

Acknowledgments

H Wadati and J Geck contributed equally to this work. The authors would like to thank Y Wakabayashi, U Staub, A Tanaka, and J Okamoto for informative discussions. This research was made possible with financial support from the Canadian funding organizations NSERC, CFI, and CIFAR and is granted by the Japan Society for the Promotion of Science (JSPS) through the 'Funding Program for World-Leading Innovative R&D on Science and Technology

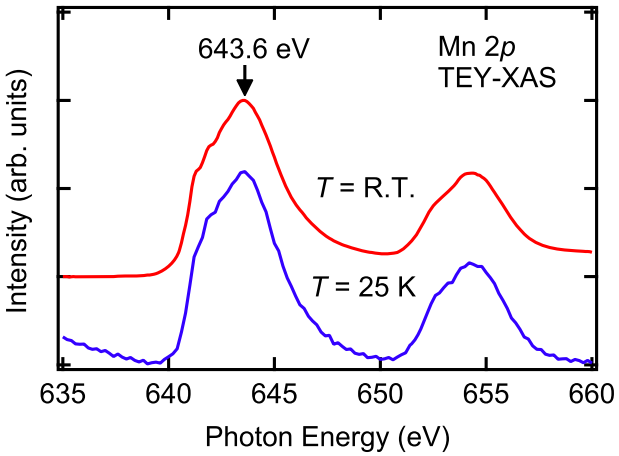

Figure B1. Mn 2*p* x-ray absorption spectrum.

(FIRST Program)', initiated by the Council for Science and Technology Policy (CSTP). This work was supported in part by JSPS Grant-in-Aid for Scientific Research(s) No. 24224009. J Geck gratefully acknowledges the support through the DFG Emmy Noether Program (Grant GE-1647/2-1). Experiments described in this paper were performed at the Canadian Light Source, which is funded by the CFI, NSERC, NRC, CIHR, the Government of Saskatchewan, WD Canada and the University of Saskatchewan.

Appendix A. Coexistence of the domains

In the paper, we referred to these twin domains as $D1$ and $D2$, respectively, and designate the reflections and directions of these domains with a corresponding index. The coexistence of the domains $D1$ and $D2$ is shown in figure A1.

Appendix B. Mn *2p* x-ray absorption spectra

Due to the large temperature dependence of the resonant x-ray diffraction, one may have expected also a large temperature dependence in the XAS. However as shown in figure B1 the XAS spectrum is basically temperature-independent. This is because the XAS is a q-integrated measurement and is not sensitive to the various phase transitions involving only spin ordering and orbital ordering. Quite different from RSXS at superlattice q vectors, XAS averages over all the sites and spin directions, while RSXS at superlattice peaks is sensitive to differences in the site and spin-dependent scattering factors.

Appendix C. Electrical resistivity and magnetization

Similarly to the XAS, we also did not observe any anomalies of electrical resistivity and magnetization at 150 K and of magnetization at 75 K, as shown in figure C1.

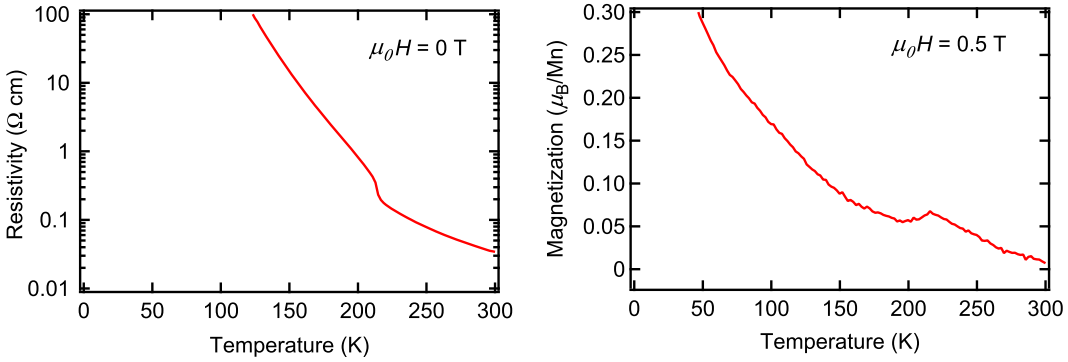

Figure C1. Electrical resistivity and magnetization.

Appendix D. Calculation of the resonant structure factor

The calculation of the structure factor for the ordered phase starts from the expressions derived in [24] for the resonant scattering length in D_{4h} and O_h symmetry. The former point symmetry is assigned to the Mn^{3+} site and the latter to the Mn^{4+} site, respectively. All 16 Mn sites within the CE unit cell are taken into account [26, 27], whereas small shifts of the lattice sites away from the high-symmetry positions and tilts are neglected. Different from the standard CE-order we assumed ferromagnetic spin correlations along the orthorhombic c direction (*Pbnm* setting).

The polarizations $\mathbf{e}_{i,f}$ and the spin directions $\hat{s}_l$ are expressed in the local coordinate system of the Mn sites given by $\mathbf{x}$, $\mathbf{y}$, $\mathbf{z}$, where $\mathbf{x}$, $\mathbf{y}$, and $\mathbf{z}$ are along the Mn–O bond directions of the octahedron and $\mathbf{z}$ is parallel to the orthorhombic c-direction. Using the unit vectors $\hat{u}_1 = (1\ \bar{1}\ 1)/\sqrt{3}$ (within the scattering plane), $\hat{u}_2 = (\bar{1}\ 1\ 2)/\sqrt{6}$ (perpendicular to the scattering plane) and $\hat{u}_3 = (1\ 1\ 0)/\sqrt{2}$ (along the scattering vector), which are also expressed referring to $\mathbf{x}$, $\mathbf{y}$, and $\mathbf{z}$, the polarization vectors of the incoming and outgoing beam are written as $\mathbf{e}_\sigma = \mathbf{e}'_\sigma = \hat{u}_2$, $\mathbf{e}_\pi = \hat{u}_1 \sin\vartheta + \hat{u}_3 \cos\vartheta$, and $\mathbf{e}'_\pi = -\hat{u}_1 \sin\vartheta + \hat{u}_3 \cos\vartheta$, where $\vartheta \simeq 60^\circ$ is the Bragg-angle of the (1/2, 0, 0)/(0, 1/2, 0) reflection at the Mn $2p$ edge.

In order to describe the orbital ordering, the resonant structure factors in D_{4h} with the C_4-axis along $\mathbf{x}$ and $\mathbf{y}$ are needed. In the specific case of $(3x^2 - r^2)/(3y^2 - r^2)$ orbital order, the C_4-axis points along the orbital, whereas in the case of $(x^2 - z^2)/(y^2 - z^2)$ orbital order, this axis is perpendicular to the occupied orbital. It is important to note here that the current analysis holds for both cases and does not depend on the specific type of orbital order. It also does not make any assumptions about the size of the charge disproportionation δ, which describes occurrence of $Mn^{3.5-\delta}$ and $Mn^{3.5+\delta}$ sites due to charge order. The model only assumes Mn sites with different symmetries.

The resonant form factors can be obtained from the expressions in [24] by calculating $\hat{f}_x(\hat{s}) = R_y \cdot \hat{f}(R_y^+ \cdot \hat{s}) \cdot R_y^+$, and $\hat{f}_y(\hat{s}) = R_x \cdot \hat{f}(R_x^+ \cdot \hat{s}) \cdot R_x^+$, where $R_x(R_y)$ describes a $\pi/2$-rotation about x (y). With these conventions we obtain for the (1/2, 0, 0) orbital order reflection:

$$\hat{F}_{orb} = 4\left(f^{(0)}_{a_{1g},A} - f^{(0)}_{a_{1g},B}\right)\begin{pmatrix}1 & 0 & 0\\ 0 & -1 & 0\\ 0 & 0 & 0\end{pmatrix} + \begin{pmatrix}\alpha(s_x, s_y, s_z, s_x) & 0 & \beta(s_x, s_z)\\ 0 & \alpha(s_y, s_x, s_y, s_z) & -\beta(s_y, s_z)\\ \beta(s_x, s_z) & -\beta(s_x, s_z) & \gamma(s_x, s_y)\end{pmatrix}$$
$$= \hat{F}^{(0)}_{orb} + \hat{F}^{(2)}_{orb}$$

with

$$\alpha(a, b, c, d) = 4f^{(2)}_{a_{1g},A}\left(a^2 - \frac{1}{3}\right) + 2f^{(2)}_{a_{1g},B}\left(b^2 - \frac{1}{3}\right) + 2f^{(2)}_{b_{1g}}(c^2 - d^2)$$
$$\beta(a, b) = 4\left(f^{(2)}_{e_g} - f^{(2)}_{b_{2g}}\right)a\,b$$
$$\gamma(a, b) = 4\left(f^{(2)}_{b_{1g}} - f^{(2)}_{a_{1g},B}\right)(a^2 - b^2)$$

This means that there is a spin-dependent contribution to the orbital ordering peak, which is given by $\hat{F}^{(2)}$. However, since we do not observe strong changes in the lineshape of I_σ below T_N, the contribution due to $\hat{F}^{(2)}$ seems to be small. For the magnetic (0, 1/2, 0) superlattice peak we obtain

$$\hat{F}_{mag} = 4\begin{pmatrix}0 & 2f^{(1)}_{e_u}s_z & -\left(f^{(1)}_{e_u} + f^{(1)}_{a_{2u}}\right)s_y\\ -2f^{(1)}_{e_u}s_z & 0 & \left(f^{(1)}_{e_u} + f^{(1)}_{a_{2u}}\right)s_x\\ \left(f^{(1)}_{e_u} + f^{(1)}_{a_{2u}}\right)s_y & -\left(f^{(1)}_{e_u} + f^{(1)}_{a_{2u}}\right)s_x & 0\end{pmatrix}$$
$$+ 4\begin{pmatrix}0 & 2f^{(3)}_{e_u}s_z\left(s_z^2 - \frac{3}{5}\right) & -\left(f^{(3)}_{e_u} + f^{(3)}_{a_{2u}}\right)s_y\left(s_y^2 - \frac{3}{5}\right)\\ -2f^{(3)}_{e_u}s_z\left(s_z^2 - \frac{3}{5}\right) & 0 & \left(f^{(3)}_{e_u} + f^{(3)}_{a_{2u}}\right)s_x\left(s_x^2 - \frac{3}{5}\right)\\ \left(f^{(3)}_{e_u} + f^{(3)}_{a_{2u}}\right)s_y\left(s_y^2 - \frac{3}{5}\right) & -\left(f^{(3)}_{e_u} + f^{(3)}_{a_{2u}}\right)s_x\left(s_x^2 - \frac{3}{5}\right) & 0\end{pmatrix}$$
$$= \hat{F}^{(1)}_{mag} + \hat{F}^{(3)}_{mag}$$

Using the above expressions, the intensity of the orbital and magnetic reflection can be calculated for given polarizations $\mathbf{e}_{i,f}$ of the incident and scattered beam: $I = \left|\mathbf{e}_f^{+} \cdot \hat{F} \cdot \mathbf{e}_i\right|^2$ with $\mathbf{e}_i = \mathbf{e}_{\sigma,\pi}$, $\mathbf{e}_f = \mathbf{e}'_{\sigma,\pi}$.

References

[1] Imada M, Fujimori A and Tokura Y 1998 *Rev. Mod. Phys.* **70** 1039
[2] Ramirez A P 1997 *J. Phys.: Condens. Matter* **9** 8171
[3] Tokura Y and Nagaosa N 2000 *Science* **288** 462

[4] Rao C N R, Arulraj A, Cheetham A K and Raveau B 2000 *J. Phys.: Condens. Matter* **12** R83
[5] Prellier W, Lecoeur P and Mercey B 2001 *J. Phys.: Condens. Matter.* **13** R915
[6] Dagotto E, Hotta T and Moreo A 2001 *Phys. Rep.* **344** 1
[7] Haghiri-Gosnet A M and Renard J P 2003 *J. Phys. D: Appl. Phys.* **36** R127
[8] Tokura Y 2006 *Rep. Prog. Phys.* **69** 797
[9] Jirak Z, Krupicka S, Simsa Z, Dlouha M and Vratislav S 1985 *J. Magn. Magn. Mater.* **53** 153
[10] Daoud-Aladine A, Rodriguez-Carvajal J, Pinsard-Gaudart L, Fernandez-Diaz M T and Revcolevschi A 2002 *Phys. Rev. Lett.* **89** 097205
[11] Efremov D V, van den Brink J and Khomskii D I 2004 *Nature Mater.* **3** 853
[12] Nakamura M, Ogimoto Y, Tamaru H, Izumi M and Miyano K 2005 *Appl. Phys. Lett.* **86** 182504
[13] Okuyama D, Nakamura M, Wakabayashi Y, Itoh H, Kumai R, Yamada H, Taguchi Y, Arima T, Kawasaki M and Tokura Y 2009 *Appl. Phys. Lett.* **95** 152502
[14] Wilkins S B, Hatton P D, Roper M D, Prabhakaran D and Boothroyd A T 2003 *Phys. Rev. Lett.* **90** 187201
[15] Dhesi S S, Mirone A, De Nadai C, Ohresser P, Bencok P, Brookes N B, Reutler P and Revcolevschi A 2004 *Phys. Rev. Lett.* **92** 056403
[16] Thomas K J *et al* 2004 *Phys. Rev. Lett.* **92** 237204
[17] Wilkins S B, Beale T A W, Hatton P D, Purton J A, Bencok P, Prabhakaran D and T Boothroyd A 2005 *New J. Phys.* **7** 80
[18] Staub U, Garcia-Fernandez M, Bodenthin Y, Scagnoli V, De Souza R A, Garganourakis M, Pomjakushina E and Conder K 2009 *Phys. Rev.* B **79** 224419
[19] Zhou S Y *et al* 2011 *Phys. Rev. Lett.* **106** 186404
[20] Wadati H *et al* 2012 *Phys. Rev. Lett.* **108** 047203
[21] Scagnoli V, Staub U, Mulders A M, Janousch M, Meijer G I, Hammerl G, Tonnerre J M and Stojic N 2006 *Phys. Rev.* B **73** 100409(R)
[22] Hawthorn D G *et al* 2011 *Rev. Sci. Instrum.* **82** 073104
[23] Thole B T and van der Laan G 1988 *Phys. Rev.* B **38** 3158
[24] Haverkort M W, Hollmann N, Krug I P and Tanaka A 2010 *Phys. Rev.* B **82** 094403
[25] SenGupta S, Wadati H and Sawatzky G A 2011 *Europhys. Lett.* **93** 47008
[26] Wollan E O and Koehler W C 1955 *Phys. Rev.* **100** 545
[27] Goodenough J B 1976 *Magnetism and the Chemical Bond* (New York: Krieger)